Two-Path Cutoff Waveguide Dielectric Resonator Filters

HIROSHI SHIGESAWA, SENIOR MEMBER, IEEE, MIKIO TSUJI, MEMBER, IEEE,
TOMOYOSHI NAKAO, AND KEI TAKIYAMA, MEMBER, IEEE

Abstract —**This paper proposes a new type of evanescent-mode waveguide filter consisting of two parallel cutoff waveguide paths with dielectric resonators. We initiate here an accurate design method incorporating both the full-wave analytical method and the impedance inverter method. The specified overall characteristic is then synthesized with the help of a computer-aided design method.**

Measurements on several kinds of filters modeled at *X*-band show excellent agreement with the designed characteristics.

I. INTRODUCTION

MICROWAVE band-pass filters employing dielectric resonators in an evanescent-mode waveguide were discussed in [1]–[3] and more recently in [4] and [5] (also, see [6] for a good summary). Such filters are operated in the cutoff region of a waveguide and have their passband in it. Therefore, if the passband center frequency f_0 is set sufficiently below the cutoff frequency f_c of a waveguide, it is easy to realize a high attenuation cutoff rate in the off-passband lower than f_0, but a relatively low insertion loss still remains in the off-passband higher than f_0. This feature is very basic to this type of filter [4].

To improve such a feature, we have proposed a new type of evanescent-mode waveguide filter [7], which consists of two parallel cutoff paths realized by a partial *H*-plane bifurcation of a rectangular waveguide. This filter can be compared with the dual-mode dielectric resonator filters [8] which exhibit elliptic behavior. This type of filter realizes intercavity couplings by means of cross slots and achieves negative coupling by using coupling screws. Therefore, we have to design such a filter by considering simultaneously both the passband and stop-band responses.

On the other hand, the new type of filter presented here achieves negative coupling by means of a subsidiary cutoff path connected in parallel with the main path. Each of the constituent paths has one or a number of dielectric resonators, and the resonant frequency of the main path is set far from that of the subsidiary path. Therefore, near the frequency of the resonant transmission of the main path, the output power from the subsidiary path makes a negligible contribution to the overall transmission characteristic, because the subsidiary path is below deep cutoff and the resonator in it is off-resonance. Then we may approximately design the passband response of a filter by fitting the main path response to the specified passband response, independent of the design of the stop-band response.

On the other hand, in the off-passband, where both paths are on the off-resonance, the output waves through both paths interfere and cancel each other at the frequencies where the condition of equal amplitude and opposite phase holds. Then such two paths can generate a filter response like that of an elliptic function band-pass filter. Therefore, we may expect to have a wide stop band with high attenuation cutoff rate even in the off-passband higher than f_0. The characteristic mentioned above reduces the design complexity of filters with multiple attenuation poles.

In Section II, we develop a design method for such a filter. As mentioned below, this type of filter includes several complicated junction discontinuities, so discontinuity problems must be solved by the full-wave analysis. To this end, we use a waveguide section partially filled with dielectric as a resonator. Of course, we may use other types of resonator (e.g., the fundamental $TE_{01\delta}$ mode in a pill-type DR) [9]. It is, however, generally difficult to consider precisely their boundary value conditions when they set up a filter in conjunction with complicated waveguide discontinuities, as discussed below. Thus, we employ simple structures as dielectric resonators.

Our approach then uses the mode-matching method, which takes into account the effect of not only the fundamental TE_{10} mode but also a large number of higher order modes generated at junction discontinuities. These results are then used to design the main path structure in cooperation with the impedance inverter method, while the subsidiary path structure is designed by a computer-aided design method so that the filter under consideration fits the specified overall characteristic.

Manuscript received August 17, 1988; revised January 26, 1989. This work was supported in part by a Grant-in-Aid for General Scientific Research from the Ministry of Education, Science and Culture, Japan (No. 63550261) and by the Murata Science Foundation.

H. Shigesawa, M. Tsuji, and K. Takiyama are with the Department of Electronics, Doshisha University, Karasuma-Imadegawa, Kamikyo-Ku, Kyoto, 602 Japan.

T. Nakao was with the Department of Electronics, Doshisha University, Kyoto, Japan. He is now with the Osaka Gas Company, Osaka, Japan.

IEEE Log Number 8927795.

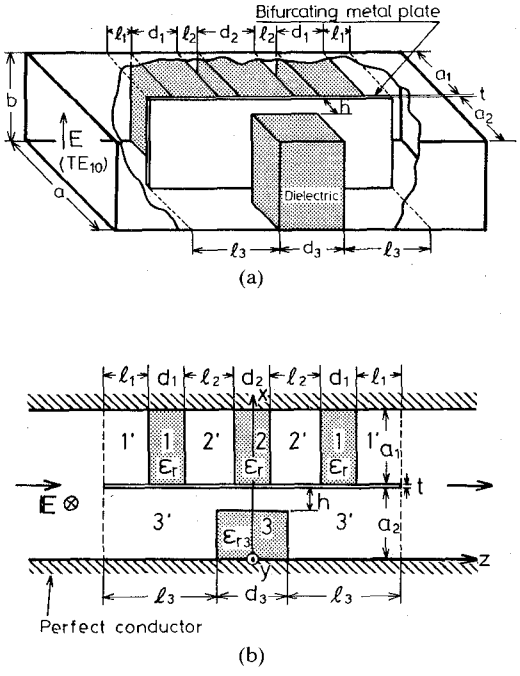

Fig. 1. (a) Sketch of an example of two-path cutoff waveguide dielectric resonator filters. (b) Top view of (a) and the dimensions.

In Section III, the practical performance aspects of this type of filter are discussed from the experimental point of view, and the effectiveness of the new filter structure and its design method is demonstrated.

II. Design Procedures

A. Full-Wave Analysis and Equivalent Network Representation

The structure under consideration is shown schematically in Fig. 1(a), which, as an example, contains three dielectric resonators in one (main path) of the bifurcated waveguides, while an additional dielectric resonator is in another subsidiary path. Fig. 1(b) shows the top view of Fig. 1(a). Each of the resonators is directly coupled with neighboring ones and/or with the input or the output waveguide through cutoff waveguide sections. As seen from Fig. 1(a), this type of filter is quite complicated in its structure when viewed as a boundary value problem of the electromagnetic fields. Therefore, the effects not only of the fundamental TE_{10} mode but also of a large number of higher order modes generated at the input and output junction discontinuities must be accurately taken into account. Such an approach leads to a generalized network representation for a filter structure, which allows us to analyze separately each of the constituent blocks shown in Fig. 1(b) (e.g., region 1′ and 1) [7], [10].

For the reason mentioned in the preceding section, we may assume that the passband response is approximately understood from the resonant transmission characteristic of the main path. In this case, the influence of the subsidiary path, of course, should be taken into account, although this path is below deep cutoff and the resonator

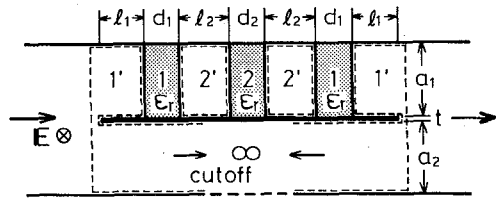

Fig. 2. Approximated filter structure for passband design, where the port at one side in the subsidiary path never sees the other side.

in it is nonresonant. Then, to a good approximation, we may replace the subsidiary path with a hypothetical homogeneous cutoff waveguide with an infinite length as shown in Fig. 2. Such an approximated structure eases a bit the complication of the full-wave analysis of the discontinuities, and these results are then effectively used for synthesizing the passband response, which is practically realized in the microwave region by the use of only series resonators and impedance inverters [11]. In the present case, each of the cutoff regions 1′ and 2′ in Fig. 2 (the approximated subsidiary path is included in region 1′ as enclosed by the dotted line) is represented by a corresponding impedance inverter network, while each of the dielectric resonators (regions 1 and 2) is replaced by a corresponding series resonator.

Region 1′ is asymmetrically sandwiched by two terminal planes of different types denoted by ① and ② in Fig. 3(a), so that the corresponding T-type lumped-element network should also be asymmetric as shown in Fig. 3(c). To derive it, the generalized scattering matrix $[S_D]$ is obtained for the discontinuity between terminal planes ① and ①′ by considering N modes at terminal plane ① on the input waveguide and N_1 ($< N$) modes at plane ①′ in the main path [10]. The residual N_2 ($= N - N_1$) modes are assigned to the ports at the terminal plane on the subsidiary path, and the boundary condition at the discontinuity plane is then solved by the mode-matching method based on the least-squares boundary residual method [7], [12].

On the other hand, the cutoff region between ①′ and ② can be equivalently represented by the uncoupled N_1 cutoff transmission line network. Here, we may understand that only a few higher order modes generated at plane ①′ barely see terminal plane ② through the cutoff transmission lines. The region behind plane ② is also below cutoff for such modes, and they never see significantly the succeeding dielectric–air interfaces. Therefore, we may arrive at a rough approximation by terminating such transmission lines with their own characteristic impedances at plane ②, while terminating the residual higher order ports with their own characteristic impedances at plane ①′.

Consequently, the equivalent network between the terminal planes ① and ② can be represented as shown in Fig. 3(b). If we look at the network of Fig. 3(b) through the only propagating TE_{10} mode at terminal ① and ②, we can finally derive an asymmetrical T-type lumped-ele-

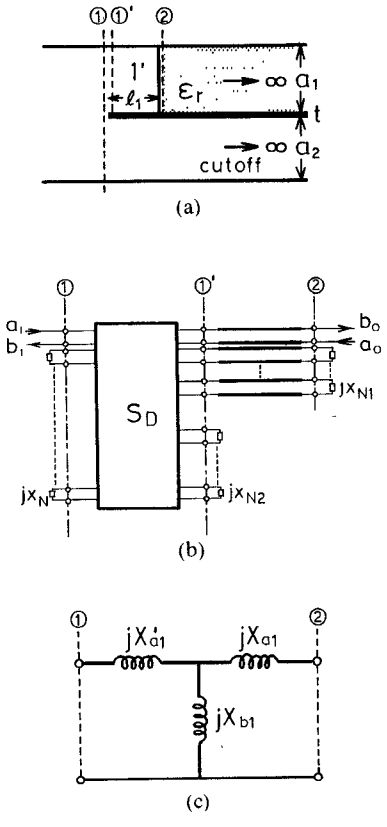

Fig. 3. (a) Cutoff section sandwiched asymmetrically by terminal planes of different type. (b) Generalized network representation for (a). (c) Asymmetrical T-type lumped-element network available for the structure in (b).

ment network as shown in Fig. 3(c) [12], which will be transformed into a corresponding impedance inverter network.

Before discussing such approaches, let us briefly consider region ②' of Fig. 2. Following the discussions mentioned above, we may neglect the effect of the higher order modes in this section. Then an existing waveguide theory [13] easily represents such a structure by a symmetrical T-type lumped-element network with the elements X_{a2} and X_{b2} in place of X_{a1} ($= X'_{a1}$) and X_{b1} in Fig. 3(c), respectively. Such a network is, of course, transformed into an impedance inverter network by following a similar approach as discussed below.

Now, let us discuss the network transformation of Fig. 3(c) into the corresponding impedance inverter network by the two approaches. The main subject of the following discussions, of course, relates to how to transform the asymmetrical network of Fig. 3(c).

In the first approach, the network of Fig. 3(c) is transformed into a symmetrical T-type network plus an accompanying shunt reactance element jX_c. The element jX_c will be canceled, at least at the passband center frequency, by devising suitable waveguide elements in practical filters (discussed in Section III). As a result, the final equivalent network for Fig. 2 can be expressed as shown in Fig. 4(a). (The shunt reactance elements are not shown here.) Now, an existing theory easily transforms Fig. 4(a) into a corresponding impedance inverter network with the parameters K and Φ as shown in Fig. 4(b) (see [14, fig. 8.03-3(a)] for detail), where

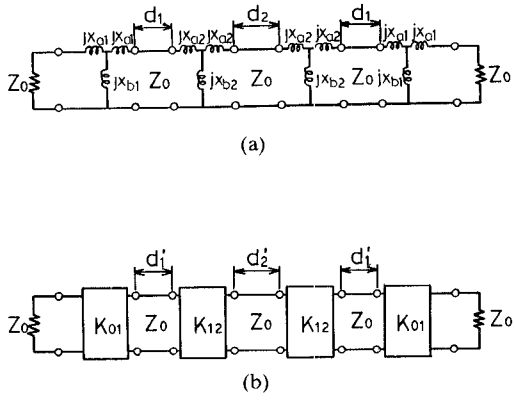

Fig. 4. (a) Equivalent network representation for the passband model of Fig. 2. (b) Network representation using impedance inverters.

$$\beta_0 d'_i = \beta_0 d_i - (\Phi_{i-1,i} + \Phi_{12})/2 \qquad (i=1,2). \quad (1)$$

β_0 is the phase constant at the passband center frequency f_0 in the region filled with the dielectric material, and (K_{01}, Φ_{01}) and (K_{02}, Φ_{12}) are obtained by replacing (X_a, X_b) in the equations of [14, fig. 8.03-3(a)] with (X_{a1}, X_{b1}) and (X_{a2}, X_{b2}), respectively. The characteristic impedance Z_0 appearing there will be discussed later on. The approach mentioned above (hereafter referred to as method I) is indeed useful for synthesizing the main path structure, but providing additional waveguide elements for canceling residual reactance elements will become a serious drawback in practice.

Contrary to method I, the second approach (referred to as method II) transforms the asymmetrical T-type network of Fig. 3(c) directly into a corresponding impedance inverter network. To this end, the additional transmission lines with the different electrical lengths $\Phi''_{01}/2$ and $\Phi'_{01}/2$ are connected to terminal ports ① and ②, respectively. As a result, the voltage–current transmission matrix $[F]$ (hereafter referred to as the fundamental matrix) of such a network can be easily expressed in conjunction with the fundamental matrix $[F_0]$ of the network of Fig. 3(c). Therefore, equating the fundamental matrix $[F]$ to that of an idealized impedance inverter network, the following inverter parameters (K'_{01}, Φ'_{01}) serve for the parameters (K_{01}, Φ_{01}) obtained by method I:

$$\begin{aligned} K'_{01} = \big|&\cos(\Phi'_{01}/2)\cos(\Phi''_{01}/2)\{A_1 Z_0 \tan(\Phi'_{01}/2) \\ &+ jCZ_0^2 \tan(\Phi'_{01}/2)\tan(\Phi''_{01}/2) - jB \\ &+ A_2 Z_0 \tan(\Phi''_{01}/2)\}\big| \end{aligned} \quad (2)$$

$$\beta_0 d'_1 = \beta_0 d_1 - (\Phi'_{01} + \Phi_{12})/2$$

$$\beta_0 d'_2 = \beta_0 d_2 - \Phi_{12} \quad (3)$$

where

$$\tan(\Phi'_{01}/2) = \{A_1 + jCZ_0 \tan(\Phi''_{01}/2)\} / \{A_2 \tan(\Phi''_{01}/2) - jB/Z_0\} \quad (4)$$

$$\tan(\Phi''_{01}/2) = \{-P \pm (P^2 - 4Q^2)\}/2Q \quad (5)$$

$$P = j(A_1 CZ_0 - A_2 B/Z_0) \quad (6)$$

$$Q = A_1^2 - A_2^2 + C^2 Z_0^2 - B^2/Z_0^2. \quad (7)$$

Here A_1, B, C, and A_2 are the matrix elements of $[F_0]$.

By the way, we may use (K_{12}, Φ_{12}) obtained by method I as the inverter parameters for region 2′ even in this case. Therefore, in following method II, we have only to replace the inverter parameters (K_{01}, Φ_{01}) with (K'_{01}, Φ'_{01}) in Fig. 4(b), and the synthesis of the main path structure can be performed without devising any additional waveguide element.

B. Approximation of Specified Passband Response

Now let us define the structural parameters determining the passband response. In general, a well-known low-pass to band-pass mapping can relate exactly the response of a low-pass prototype circuit to that of a corresponding band-pass circuit. Then, following the standard design approach [11], [14], one can easily solve the reactance element values g_n $(n = 0, 1, \cdots, n+1)$ of the low-pass prototype circuit (see [14, fig. 8.02-2(a)]) so as to realize the specified passband response (a maximally flat characteristic, a Chebyshev characteristic, etc.). Such a lumped-element circuit is much more practically converted in the microwave region by the use of only series resonators and impedance inverters as mentioned before (or see [14, fig. 8.02-2(c)]), and the impedance parameters can then be derived as follows:

$$K_{i,i+1}/Z_0 = T/(g_i g_{i+1})^{1/2} \qquad (i = 0, 1) \quad (8)$$

where

$$T = (\pi \lambda_{g0}/2\omega'_1)(1/\lambda_{g2} - 1/\lambda_{g1})$$
$$g_0 = T \qquad g_2 = T/r_L. \quad (9)$$

Here λ_{g0}, λ_{g1}, and λ_{g2} denote, respectively, the guide wavelengths at f_0 and at the lower and upper passband edge frequencies; r_L represents the load resistance of the band-pass ladder network corresponding to the low-pass prototype filter, of which the passband edge or equal-ripple band edge is ω'_1. Thus, equating K_{01} and K_{12} of method I or K'_{01} and K_{12} of method II to the values given by (8), respectively, one can formally solve for the necessary dimensions l_1 and l_2 (see Fig. 2) of regions 1′ and 2′, respectively.

To finish this completely, it is necessary to define the characteristic impedance Z_0 of regions 1 and 2. For the characteristic impedance of the input and output waveguides of width a, we shall assume for convenience that it is equal to the ratio of the modal voltage to the axial current as follows:

$$Z_0 = \omega_0 \mu_0 \lambda_{g0}(b/4a). \quad (10)$$

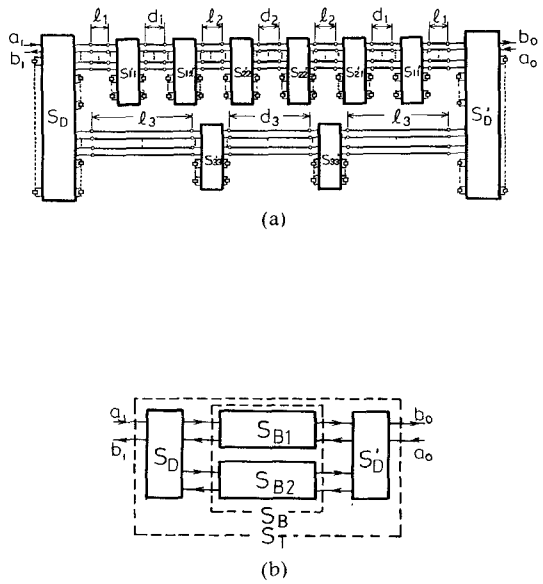

Fig. 5. (a) Generalized network representation available for any frequencies. (b) Simplified network for (a).

The width a_1 of the bifurcation should then be defined so that the characteristic impedance of region 2 is equal to that of (10), because of the necessity of keeping the symmetrical nature of an impedance inverter network. Thus, we have

$$a_1 = a/\sqrt{\epsilon_r}. \quad (11)$$

On the other hand, at the passband center frequency f_0, each of the transmission lines with length d'_i of Fig. 4(b) should exhibit the same type of resonance with the corresponding series resonator. Therefore, the electrical lengths given by (1) and (3) must be π radians, which give the necessary thicknesses d_1 and d_2 of dielectric resonators in the main path (see Fig. 2).

C. Approximation of Specified Stop-Band Response

The off-passband response of the present filter is determined by the interference between two waves passing through both paths. If the resonant transmission frequency f_{r1} due to the first higher order mode (axially odd mode) in the subsidiary path is set higher than f_0, a phase difference of about π radians between two waves can be expected in the frequency range between f_{r1} and f_{r2} (the resonant transmission frequency due to the second higher order axial mode). Therefore, if we control d_3, h, and ϵ_{r3} of Fig. 1, we can realize, at least, two attenuation poles at $f_{\infty 1}$ and $f_{\infty 2}$ in that frequency range, thereby obtaining a large insertion loss with a high attenuation rate over a wide frequency range.

To this end, the complicated wave behavior in both paths in the off-passband must be solved by the full-wave analysis [14]. After obtaining an equivalent network like Fig. 3(b) for each of the discontinuities in Fig. 1, a complete equivalent network available for the off-passband is obtained as shown in Fig. 5(a), which is transformed into a simplified network representation as shown in Fig. 5(b) [7],

[10]. After some laborious calculations [12], omitted here due to the limited available space, one can derive the matrix element S_{21}^T of the overall scattering matrix $[S^T]$ corresponding to the network of Fig. 5.

Substituting the parameters of the main path, l_i, d_i $(i=1,2)$, a_1, and ϵ_r, defined in the preceding section, and knowing the thickness of the bifurcating metal plate t in advance, the matrix element S_{21}^T becomes a function of a set of unknown parameters χ and frequency f, which defines the insertion loss L as follows:

$$L = g(f, \chi) \tag{12}$$

where

$$\chi = (\epsilon_{r3}, d_3, h). \tag{13}$$

Then, the insertion loss function given by (12) should be fit to the specified stop-band response which, for example, gives the minimum insertion loss $L_{\min}$ in the frequency range $f_{s1} \leqq f \leqq f_{s2}$. This paper accomplishes such a task by a CAD method using the following error functions:

$$G_1 = W_1 |g(f_{s1}, \chi) - L_{\min}| \tag{14}$$

$$G_2 = W_2 |g(f_{s2}, \chi) - L_{\min}| \tag{15}$$

$$G_3 = W_3 |\min_F g(f, \chi) - L_{\min}| \tag{16}$$

where W_i $(i=1 \sim 3)$ are the positive weighting constants and $F = \{f | f_{s1} \leqq f \leqq f_{s2}\}$. Although all these error functions ideally must be zero, our practical method meets these conditions within the convergence value (usually 10^{-6} or less) by using the nonlinear optimization procedure (Gauss–Marquardt method). If an obtained set χ_{root} of the parameters is physically realizable, our approximation is then finished.

Here, it should be noted that the present design method is a sequential one in which the passband is first designed by using the model shown in Fig. 2 and then the stop band is fit to the specified one by using the different model shown in Fig. 5. Therefore, a change of χ inevitably affects, to a greater or lesser degree, the passband characteristic already defined. However, such an effect is negligibly small in the present case, as seen afterward, and we do not consider any compensation.

III. Design Examples and Experiments

Let us consider the following specifications:

Passband response:	3-poles, 0.1 dB Chebyshev
Center frequency:	$f_0 = 9.5$ GHz
Bandwidth:	$\Delta f_0 = 0.3$ GHz
Fixed attenuation pole or stop band edge:	$f_{\infty 1}$ or $f_{s1} = 11.0$ GHz
Minimum insertion loss in the stopband:	$L_{\min} = 50$ dB.

Fused quartz ($\epsilon_r = 3.78$) was used for all the dielectric resonators, so that the bifurcation of the standard X-band waveguide ($a = 2.29$ cm) according to (11) results in $a_1 = 1.18$ cm. The junction discontinuities were analyzed by the mode-matching method with 60 modes in all by considering a thickness $t = 0.02$ cm of the bifurcating metal plate.

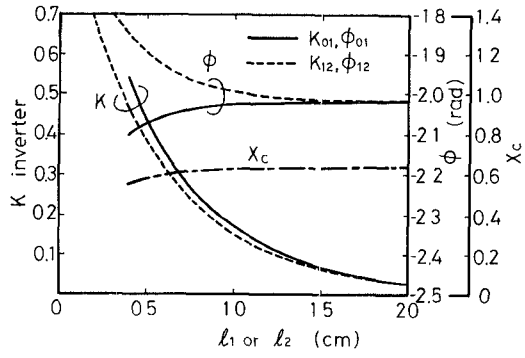

Fig. 6. Relation of the inverter parameters and the reactance element to be canceled versus the length of the cutoff waveguide section (region 1′ or 2′).

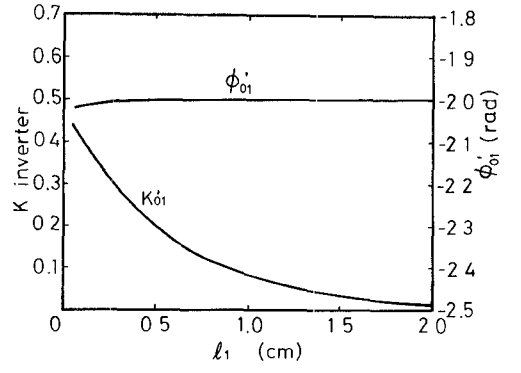

Fig. 7. Relation of the inverter parameters versus the length of region 1′, which is used in method II.

First, let us design such a filter by method I. Fig. 6 shows the relations of the inverter parameters and the reactance element to be canceled versus the length l_1 or l_2 of cutoff region 1′ or 2′. The necessary impedance inverter parameters to realize the specified passband response are calculated as $K_{01} = 0.3063$ and $K_{12} = 0.0844$ from (8), which suggest lengths $l_1 = 0.69$ cm and $l_2 = 1.33$ cm. Then Φ_{01}, Φ_{12}, and the normalized X_c values corresponding to each of those lengths result in $d_1 = d_2 = 0.4$ cm and $X_c = 0.6165$.

On the other hand, method II leads an additional relation of the inverter parameters (K'_{01}, Φ'_{01}) versus l_1 as shown in Fig. 7. In this case, the necessary impedance parameter is $K'_{01} = 0.3$, while K_{12} remains unchanged. Then the Φ'_{01} value corresponding to the suggested length $l_1 = 0.27$ cm results in $d_1 = 0.4$ cm. Since a large K value is desirable to widen the passband and make the passband ripple small, method II seems to be slightly inferior to method I with regard to this point, but there is a serious drawback in method I, as mentioned previously or as seen below.

Next, let us design the stop-band response. If a simplified approach with $h = 0$ is applied, fixing an attenuation

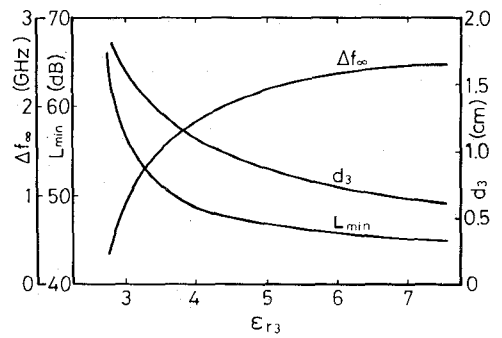

Fig. 8. Dependence of d_3, $L_{\min}$, and $\Delta_{f\infty}$ on ϵ_{r3} when $f_{\infty 1}=11.0$ GHz is specified.

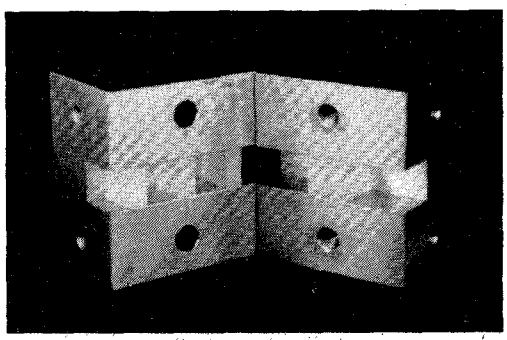

Fig. 9. Photograph of designed filter.

pole at $f_{\infty 1}=11.0$ GHz results in a definitive relation between ϵ_{r3} and d_3, which automatically defines another attenuation pole $f_{\infty 2}$ and $L_{\min}$ through a CAD program (the weighting factors W_i in (14)–(16) are set to unity for convenience). These results are shown in Fig. 8, which suggests the values $\epsilon_{r3}=3.68$ and $d_3=1.25$ cm to conform to the specified stop-band characteristic. However, we have to use $\epsilon_{r3}=3.78$ in experiments, thereby resulting in the value $d_3=1.22$. This in turn gives $L_{\min}=49.4$ dB, 0.6 dB smaller than the specified value and the corresponding $\Delta f_\infty = f_{\infty 2}-f_{\infty 1}=1.68$ GHz.

Fig. 9 gives an external view of one of the test filters, where the bifurcated waveguides loaded with dielectric resonators are opened to reveal the inside, removing the bifurcating metal plate. The reactance element (symmetrical capacitive window [13] is not shown here) is loaded half a wavelength away from the input and output discontinuity planes.

The measured results are shown in Fig. 10. The designed parameters are displayed in Fig. 10(a), where the measured insertion loss (the solid curve) shows a residual insertion loss of about 0.4 dB in the passband as shown in Fig 10(b) and its response is a bit wider than the theoretical one (the dotted curve). By the way, our setup measures the insertion loss only up to 55 dB, but roughly estimates the minimum reflection loss as about 18 dB. The sharp dips seen at around $f_{r0}=8.1$ GHz and $f_{r1}=10.9$ GHz are the series resonances corresponding to the dominant and the first higher order axial modes, respectively, in the subsidiary path. These resonances, especially at f_{r1}, play an important

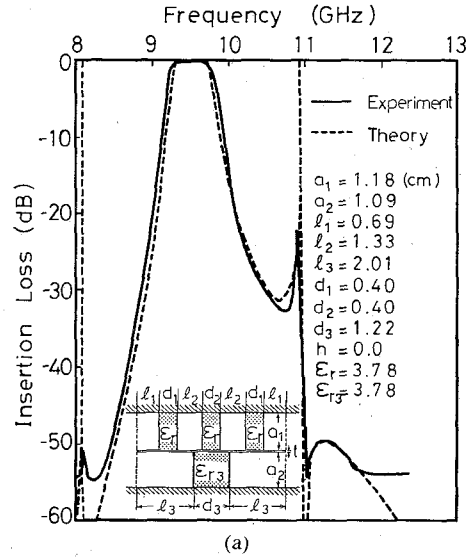

(a)

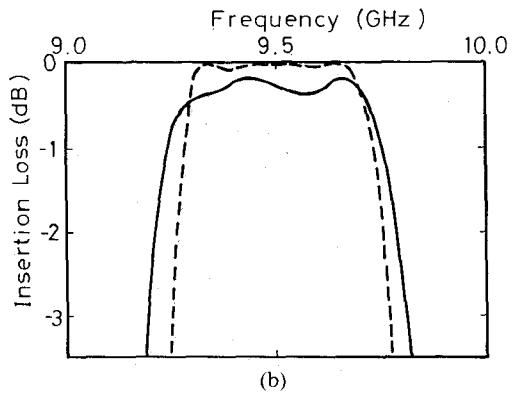

(b)

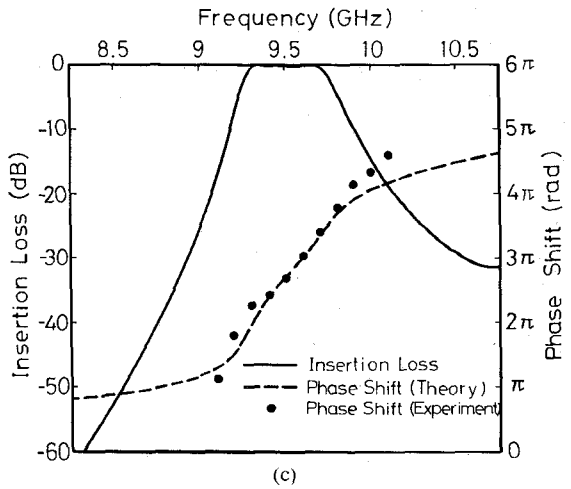

(c)

Fig. 10. (a) Measured response of the filter designed by method I with $h=0$. (b) Response around the passband. (c) Phase characteristic.

role in producing the stop-band response seen in, for example, an elliptic function filter. Fig. 10(c) shows the phase characteristic. These results show that the experimental and theoretical results are in good agreement except near the passband edge frequencies. Such discrepancies between two curves will be caused by the effects of the handmade capacitive windows, the gap between dielectrics and waveguide walls, etc.

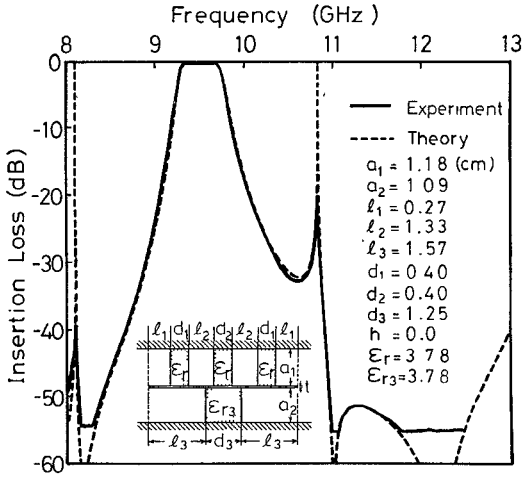

Fig. 11. Measured response of the filter designed by method II with $h = 0$.

On the other hand, Fig. 11 shows the experimental results of the filter designed by method II, but with $h = 0$. In this case, the inverter parameters are obtained by using both Fig. 6 and Fig. 7 for the prescribed values of $\epsilon_r = \epsilon_{r3} = 3.78$, $a = 2.29$ cm, and $a_1 = 1.18$ cm. The designed parameters are displayed in the figure, and the theoretical and experimental results exhibit surprisingly good agreement, perhaps because complicated capacitive windows are not used. Finally, Fig. 12(a) shows the results when the stop-band response is designed by method II with $h \neq 0$. In this case, we have full flexibility for fitting the stop-band response to the specified one by using (14), (15), and (16), into which $f_{s1} = 11.0$ GHz and $f_{s2} = 12.3$ GHz are substituted, instead of the only specifying value $f_{\infty 1}$ in the case where $h = 0$. The values ϵ_r, ϵ_{r3}, a, and a_1 are the same as in Fig. 11. The obtained parameters are displayed in the figure, and it is obvious that these results are in excellent agreement, although residual insertion loss of about 0.4 dB remains in the passband, as seen in Fig. 12(b). Incidentally, the minimum reflection loss is roughly estimated to be 20 dB.

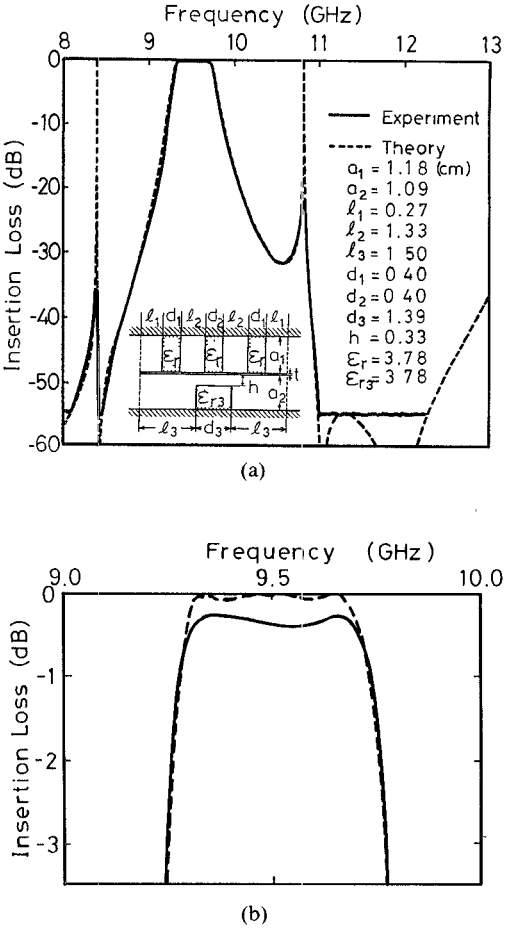

Fig. 12. (a) Measured response of the filter designed by method II with a finite h. (b) Response around the passband.

IV. Conclusions

A new type of evanescent-mode waveguide filter has been presented. A different kind of approximate design method was outlined incorporating both the full-wave analytical method and the usual impedance inverter method. Applications were made to 3-pole Chebyshev band-pass filters at *X*-band, and the results were compared with those obtained experimentally.

As mentioned above, it is necessary to have a large K value if a wide passband and a small passband ripple are desired. To realize such a value, it is obvious from Figs. 6 and 7 that the lengths l_1 and l_2 of the cutoff regions 1′ and 2′ become quite short, especially l_1. Furthermore, the variation of K is very sensitive to changes in l_1 in its short range, and the DR waveguide mixed type of our filter may have a tendency to suffer the effect of temperature deviation. This will limit the available frequency ranges of this filter to those up to about *Ka*-band. Another type of two-path cutoff filter is now being considered to improve this feature, and will be reported in another paper.

References

[1] G. F. Craven, "Waveguide bandpass filters using evanescent modes," *Electron Lett.*, vol. 2, pp. 251–252, July 1966.

[2] G. F. Craven and C. K. Mok, "The design of evanescent mode waveguide bandpass filters for a prescribed insertion loss characteristic," *IEEE Trans. Microwave Theory Tech.*, vol. MTT-19, pp. 295–308, Mar. 1971.

[3] R. V. Snyder, "New application of evanescent mode waveguide to filter design," *IEEE Trans. Microwave Theory Tech.*, vol. MTT-25, pp. 1013–1021, Dec. 1977.

[4] Y. C. Sieh and K. G. Gray, "Analysis and design of evanescent-mode waveguide dielectric resonator filters," in *1984 IEEE MTT-S Int. Microwave Symp. Dig.*, May 1984, pp. 238–239.

[5] P. Guillon, M. P. Chong, and Y. Garault, "Dielectric resonator band pass filter with high attenuation rate," in *1984 IEEE MTT-S Int. Microwave Symp. Dig.* May 1984, pp. 240–242.

[6] G. F. Craven and R. F Skedd, *Evanescent Mode Microwave Components*. Boston: Artech House, 1987, chs. 1, 3, and 4.

[7] H. Shigesawa, M. Tsuji, and K. Takiyama, "Two-path cutoff waveguide dielectric resonator filters," 1985 *IEEE MTT-S Int. Microwave Symp. Dig.*, June 1985, pp. 357–360.

[8] S. J. Fiedziusko,"Dual mode dielectric resonator loaded cavity filters," *IEEE Trans. Microwave Theory Tech.*, vol. MTT-30, pp. 1311–1316, Sept. 1982.

[9] D. Kajfez and P. Guillon, Eds., *Dielectric Resonators*. Dedham, MA: Artech House, 1986, ch. 9.
[10] H. Shigesawa, M. Tsuji, and K. Takiyama, "Two-path cutoff waveguide resonator filters with attenuation poles," in *1986 IEEE MTT-S Int. Microwave Symp. Dig.*, June 1986, pp. 407–410.
[11] S. B. Cohn, "Direct-coupled-resonator filters," *Proc. IRE*. vol. 45, pp. 187–196, Feb. 1957.
[12] T. Nakao,"A study of two-path cutoff-waveguide dielectric resonator filters," M. S. thesis, Doshisha University, Kyoto, Japan, 1987.
[13] N. Marcuvitz, *Waveguide Handbook*. New York: McGraw-Hill, 1951, sec. 5.1.
[14] G. L. Matthaei, L. Young, and E. M. T. Jones, *Microwave Filters, Impedance-Matching Networks, and Coupling Structures*. New York: McGraw-Hill, 1964, ch. 8.

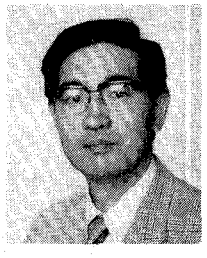

Hiroshi Shigesawa (S'62–M'63–SM'85) was born in Hyogo, Japan, on January 5, 1939. He received the B.S., M.S., and Ph.D degrees in electrical engineering from Doshisha University, Kyoto, Japan, in 1961, 1963, and 1969, respectively.

Since 1963, he has been with Doshisha University. From 1979 to 1980, he was a Visiting Scholar at the Microwave Research Institute, Polytechnic Institute of New York, Brooklyn, NY. Currently, he is a Professor in the Faculty of Engineering, Doshisha University. His present research activities involve millimeter- and submillimeter-wave guiding structures and devices and scattering problems of electromagnetic waves.

Dr. Shigesawa is a member of the Institute of Electronics, Information and Communication Engineers (IEICE) of Japan, the Institute of Electrical Engineers (IEE) of Japan, and the Optical Society of America (OSA).

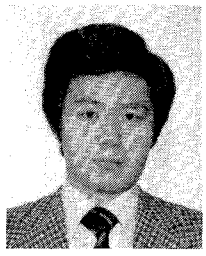

Mikio Tsuji (S'77–M'82) was born in Kyoto, Japan, on September 10, 1953. He received the B.S., M.S., and Ph.D. degrees in electrical engineering from Doshisha University, Kyoto, Japan, in 1976, 1978, and 1985, respectively.

Since 1981, he has been with Doshisha University, where he is now an Assistant Professor. His research activities have been concerned with millimeter- and submillimeter-wave guiding structures and devices.

Dr. Tsuji is a member of the Institute of Electronics, Information and Communication (IECE) of Japan.

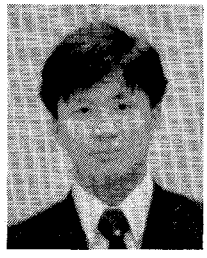

Tomoyoshi Nakao was born in Hyogo, Japan, on August 19, 1962. He received the B.S. and M.S. degrees in electrical engineering from Doshisha University, Kyoto, Japan, in 1985 and 1987, respectively. He is now with the Osaka Gas Company.

Mr. Nakao is a member of the Institute of Electronics, Information and Communication (IECE) of Japan.

Kei Takiyama (M'58) was born in Osaka, Japan, October 20, 1920. He received the B.S. and Ph.D degrees in electrical engineering from Kyoto University, Kyoto, Japan, in 1942 and 1955, respectively.

Since 1954, he has been a Professor of Electronic Engineering at Doshisha University, Kyoto, Japan, where he has carried out research in the fields of microwave transmission lines and optical engineering. From 1957 to 1958, he was a Fulbright Scholar and a Research Associate at the Microwave Research Institute, Polytechnic Institute of Brooklyn, New York.

Dr. Takiyama is a member of the Institute of Electronics, Information and Communication Engineers (IEICE) of Japan, the Institute of Electrical Engineers (IEE) of Japan, and the Optical Society of America (OSA).